Unified Modulation Pattern Analysis (UMPA) algorithm for 1D sensitive X-ray phase contrast imaging techniques

V. Di Trapani,[a,b,*] **L. Brombal,**[a,c] **F. De Marco,**[a,b] **D. Dreossi**[b] **and P. Thibault**[a,b]

[a] *Department of Physics,University of Trieste, Via A. Valerio 2, Trieste, Italy*

[b] *Elettra-Sincrotrone Trieste, Strada Statale 14 — km 163.5, 34149 Basovizza (Trieste) Italy*

[c] *National Institute for Nuclear Physics (INFN), Division of Trieste, Via. A. Valerio 2, 34127 Trieste, Italy*

E-mail: vittorio.ditrapani@units.it

Abstract: X-ray phase contrast imaging (XPCI) techniques are sensitive to refraction (differential-phase) and small-angle X-ray scattering (dark-field) signals, not measurable with conventional absorption imaging techniques. Among XPCI techniques, edge illumination (EI), grating interferometry (GI), and speckle-based imaging (SBI) make use of wavefront markers, such as absorbing masks with periodical apertures or random diffusers, to encode refraction and dark-field signals induced by the sample. The Unified Modulated Pattern Analysis (UMPA) provides an algorithmic solution to extract the transmission, refraction, and dark-field images from EI, GI, and SBI datasets where the wavefront marker is directly resolved by the employed detection system. In its original implementation, UMPA has been designed for XPCI techniques sensitive to refractions along two axes. This work presents a modified version of the algorithm to extend its applicability to all the existing XPCI techniques that use wavefront markers with sensitivity to refraction limited along one direction (UMPA-1D). The algorithm, written in C++ and Cython and parallelized with OpenMP, enables fast reconstruction times that are particularly convenient for large tomographic datasets. The validity of the UMPA-1D has been demonstrated using both simulated images and real acquisitions with an EI setup in beam-tracking mode.

Keywords: Multi-modality systems; Simulation methods and programs; X-ray radiography and digital radiography (DR)

*Corresponding author.

Contents

1 Introduction

X-ray phase-contrast imaging (XPCI) is an umbrella term including all the techniques which allow extracting the phase and small-angle scattering signals inaccessible to conventional absorption X-ray imaging [1]. Among XPCI techniques, differential-phase techniques are based on the measurement of the refraction induced by the sample, which is proportional to the gradient of the phase shift (differential phase image). By integrating the differential phase image, it is then possible to obtain the 2D map of phase signals (integrated phase image), which, if compared with conventional transmission images, improves the visibility of weakly absorbing materials, such as biological tissues. Additionally, several XPCI techniques allow for the extraction of the small-angle X-ray scattering (dark-field) signal, which allows visualizing features in the sample with sizes not resolvable by the employed detection system [2].

Among XPCI techniques, edge illumination (EI) and grating interferometry (GI) make use of one or more absorbing masks featuring periodically repeated apertures, which encode refraction and dark-field induced by the sample [3, 4]. A different approach to the use of absorbing masks is provided by speckle-based imaging (SBI). This latter technique uses a partially coherent X-ray beam and randomly distributed scatterers (such as silicon-carbide grits in sandpapers) to create a reference speckle pattern at the detector position [5]. In the usual setups for EI, GI, and SBI, the refraction and the dark-field signals are extracted by comparing the images of the wavefront markers (masks or speckles) before and after the introduction of a sample in the field of view.

Several algorithms have been proposed to extract the phase information from datasets acquired with EI, GI, or SBI setups. However, many are application-specific, computationally expensive, and possibly time-consuming [5–7]. Among these algorithms, the Unified Modulation Pattern Analysis (UMPA) uses a template matching approach where a least squares minimization of a model, including transmission, refraction, and the dark-field signal, is carried out for each pixel in the images within a user-defined neighborhood [8]. A new version of UMPA, written in C++ and

Cython, and parallelized with OpenMP, has been recently implemented with the main advantage of being up to 120× faster than the previous version implemented in Python [9].

Though the SBI technique has an intrinsic 2D sensitivity to refraction angles, the sensitivity of EI or GI depends on the structure of the mask, which can be 1D (e.g., a bar pattern with a fixed period) or 2D (e.g., a grid with fixed period both along the vertical and horizontal axes). The original version of UMPA was designed to track and measure refraction in both horizontal and vertical axes. As a result, it tends to be unreliable when applied to XPCI techniques sensitive to refraction only along one direction, making use of 1D masks. However, it is worth noting that 2D sensitivity to refraction can also be achieved with 1D masks by implementing tailored setups/acquisition procedures, e.g., acquiring multiple images by rotating the mask around the optical axis [8].

In this work, we present a modified version of UMPA to extend its applicability to the cases where masks with 1D periodicity are employed (UMPA-1D). This 1D version of UMPA has been tested for an EI setup in beam-tracking mode, i.e., where a detector resolving a single mask with 1D periodicity is employed [6]. For these setups, a complete dataset (i.e., full illumination of the sample) can be obtained by acquiring multiple reference/sample images with different relative lateral displacements between the mask and the sample. This is usually achieved by mounting the mask (or the sample) on a motorized translation stage.

The algorithm has been tested and characterized with simulated images for a beam-tracking EI setup. Finally, the algorithm was applied to experimental data of a plant specimen acquired with a synchrotron filtered white-beam and a high-resolution detection system.

2 Materials and methods

2.1 UMPA-1D algorithm

UMPA is a template-matching algorithm that extracts transmission, phase, and dark-field signals by comparing the images of a reference pattern acquired with and without a sample, here called "sample image" and "reference image". In its original implementation [8, 9], the algorithm can be applied to any diffuser (e.g., masks, sandpapers, random diffusers) and acquisition procedure that provide a 2D sensitivity to refraction. However, 1D-sensitive diffusers/acquisition procedures are widely employed. In this work, we introduce a modified version of the algorithm to extend its applicability to diffusers and acquisition procedures with 1D sensitivity to refraction.

As defined in [8], for a pixel (x, y), the intensity of the pattern recorded in the sample image $I(x, y)$ can be expressed as a function of the undistorted reference pattern in $I_0(x, y)$ as follows:

$$I^{\text{model}}(x, y) = T(x, y) \cdot \{\langle I_0(x + u, y)\rangle + D(x, y) \cdot [I_0(x + u, y) - \langle I_0(x + u, y)\rangle]\} \tag{2.1}$$

where $\langle I_0(x + u, y)\rangle$ is the average signal, $T(x, y)$ is the transmission through the sample, u is the horizontal displacement originating from refraction, and $D(x, y)$ is the visibility associated with the dark-field signal.

UMPA-1D uses an analysis window W $(2N+1)\times(2N+1)$, with N adjustable by the user. In the sample image, the window W is centered in a pixel of interest p_i, while in the reference image, several windows in the neighborhood of p_i are evaluated to find the best match between the sample and the reference image. For each pixel in the sample image, the algorithm implements a least-squares routine that computes a cost function landscape $\mathscr{L}(x,y)$ based on the model defined by eq. (2.1). In this formulation, the cost function is defined as follows:

$$\mathscr{L}(x,y;u,T,D)=\sum_{m=1}^{M}\sum_{w_x=-N}^{N}\sum_{w_y=-N}^{N}\Gamma(w_x,w_y)\cdot|I_m^{\text{model}}(x+w_x,y+w_y;u,T,D)-I_m(x,y)|^2 \qquad (2.2)$$

In eq. (2.2), the sum over w stands for the sum of the values over the analysis window, M is the number of the acquired reference positions, and $\Gamma(w_\text{x},w_\text{y})$ is a 2D Hamming window that smoothly decreases the weights of pixels close to the edges of the considered window.

The optimal match is then found for the window displacement where the cost function has its minimum. The minimization of the cost function is carried out in two steps. First, the values of T_min and D_min that minimize the cost function landscape $\mathscr{L}(x,y;u,T,D)$ at different integer shifts u are computed by setting $\partial\mathscr{L}/\partial T=\partial\mathscr{L}/\partial D=0$, and solving analytically for T and D. In a second step, the discrete lateral displacement for which $\mathscr{L}(x,y;u,T_\text{min},D_\text{min})$ has its minimum is determined with a simple heuristic method that, starting from $u=0$, compares the value of the cost function in u with its nearest neighbors, moving with discrete steps of one pixel towards the minimum value until the first local minimum for the cost function is found.

The procedure described above determines the integer shift (in pixel units) for which the cost function has its minimum. In order to find the sub-pixel minimum, the cost function landscape is approximated as a 1D parabola in the neighborhood of the local integer minimum. In particular, by setting to 0 the abscissa of u_min, the relative sub-pixel shift is calculated by fitting a parabola of equation $y=ax^2+bx+c$ using 3 points: $[x_1=-1,y_1=\mathscr{L}(u_\text{min}-1,y,T_\text{min},D_\text{min})]$, $[x_2=0,y_2=\mathscr{L}(u_\text{min},y,T_\text{min},D_\text{min})]$, and $[x_3=1,y_3=\mathscr{L}(u_\text{min}+1,y,T_\text{min},D_\text{min})]$. From a direct solution of a parabola through three points, the following values for a, b, and c are obtained: $a=0.5y_1-y_2+0.5y_3$, $b=-0.5y_1+0.5y_3$, $c=y_2$. The sub-pixel minimum of the cost function landscape is, therefore, the x-coordinate of the vertex of the fitted parabola, i.e., $u_\text{sub}=-b/(2a)$. The overall shift is finally calculated as $u_\text{min}=u_d+u_\text{sub}$ with sub-pixel precision.

2.2 Simulations

The algorithm has been tested and optimized with simulated data for an EI setup in beam-tracking mode. The simulation is based on the Fresnel angular spectrum diffraction formula for a monochromatic plane wave disturbed by the complex field introduced by the sample and propagating across the source-detector axis [10, 11].

The simulation considers an ideal detector with 4.0 µm pixels, and a Gaussian point spread function with FWHM = 2.5 pixels. Photons with energy $E=21$ keV were considered together with a propagation distance of $z=40$ cm. The sample is a sphere of SiO_2 with a radius of 750 µm. In the simulations, the mask has been modeled as a periodic 1D bar pattern with $\Delta X=20$ µm aperture,

$\Pi = 120\,\mu m$ period, and absorbing septa made by a $15\,\mu m$ thick gold layer. Finally, Poissonian noise with standard deviation $\sigma = \sqrt{\gamma}$ was added to the images, with γ the number of collected photons per pixel per image.

The ground truth was computed from phase and amplitude of the propagated wave, disturbed only by the sample, i.e., excluding the mask.

The simulated data were employed to test the effectiveness of the algorithmic implementation of UMPA-1D. Additionally, simulated datasets were produced to perform an optimization study for the choice of the step size dx for the horizontal displacements of the mask. Finally, the performance of the algorithm and the acquisition/reconstruction parameters were evaluated using the universal quality index (UQI) [12] as the figure of merit to compare the reconstructed images with the ground truth. The UQI is an objective metric that ranges from -1 to 1, whereby UQI = 1 indicates a perfect match between the compared images.

2.3 Experimental acquisitions

Images of a plant specimen were acquired with a beam-tracking EI setup implemented at the SYRMEP beamline of the Elettra synchrotron (Trieste, Italy), using a polychromatic filtered white-beam with an effective photon energy of 21 keV.

For this setup, a single mask featuring a bar pattern with apertures of $19\,\mu m$ and $116\,\mu m$ period was employed together with a detection system composed of a qCMOS camera (ORCA-Quest, Hamamatsu Photonics) mounted into an X-ray microscope system made by a high numerical aperture optics coupled with a $45\,\mu m$ thick GGG:Eu scintillator. For the scope of the acquisitions, the optics were adjusted to achieve an effective pixel size of $4\,\mu m$ to directly resolve the mask in the acquired images. The propagation distance was about 40 cm. The mask was mounted onto a translation stage. A complete dataset was collected by translating the mask over 13 diffuser positions in steps of $8.9\,\mu m$.

3 Results

As a first demonstration, a simulated dataset of sample and reference images, composed of 12 images acquired by horizontally translating the mask with steps $dx = 10\,\mu m$, was reconstructed with a (3×3) UMPA-1D reconstruction window. The simulation was carried out considering a parallel beam with uniform intensity, yielding 10^4 photons per pixel per frame. Figure 1 compares the ground truth maps of transmittance (T) and refraction (u) with the UMPA-1D reconstructed pairs.

The right column in figure 1 shows the residuals obtained by subtracting the ground truth images with their relative UMPA-1D reconstructed pair. Referring to the residual images, it can be observed that appreciable deviations from the ground truth are limited to the edges of the sphere. Additionally, from a visual inspection, it can be noted that, if compared to the transmission image, the shift image (u) features more evident deviations from the ground truth.

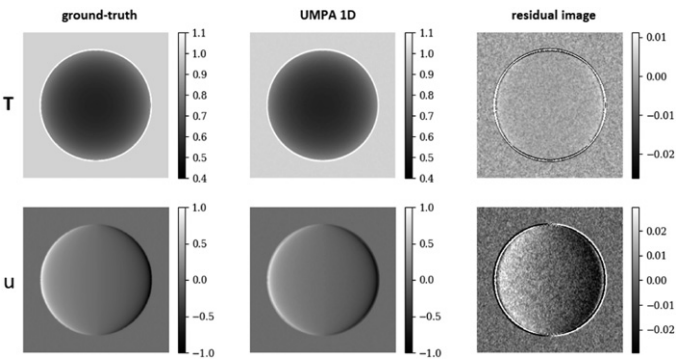

Figure 1. Comparison between ground truth and UMPA-1D (T and u) reconstructed images of a SiO_2 sphere with 750 µm radius. The right column shows the residual images, i.e., the subtraction between ground truth and UMPA-1D pairs.

Considering a mask with period Π and aperture ΔX, a complete dataset for which the sample is entirely illuminated is obtained by horizontally translating the reference mask m times, where $m \geqslant \Pi/\Delta X$ and the translation step is $\mathrm{d}x = \Pi/m$. As an example, when the translation step is larger than the apertures in the mask, parts of the sample are not illuminated, resulting in an undersampled illumination. On the contrary, for $\mathrm{d}x < \Delta X$, the beamlets generated by the apertures in the mask partially overlap, resulting in an oversampled illumination. Like most phase-retrieval algorithms, UMPA benefits from redundancies in the acquisition procedure. Therefore, an oversampled dataset is expected to improve the final image quality.

To evaluate the impact of the acquisition sampling, simulations were performed by varying the number of steps m and step size $\mathrm{d}x$. In order to compare images with the same photon statistics, for each simulated dataset, the total amount of photons/pixel was kept constant. Different datasets of reference and sample images were simulated starting from $\mathrm{d}x = 1$ µm ($\Delta X/20$) to $\mathrm{d}x = 20$ µm (ΔX). Each dataset was reconstructed with different window sizes set in the UMPA algorithm. For each reconstructed image, the UQI was evaluated by comparing the reconstructed images with the ground truth. Figure 2 shows the plots of the UQI under different conditions of window size and step sizes $\mathrm{d}x$.

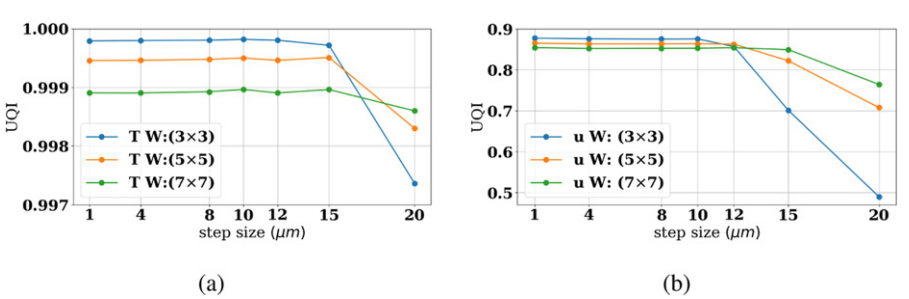

Figure 2. Plots of UQI as a function of the step size $\mathrm{d}x$, for different sizes of the analysis window in UMPA-1D: (a) transmission image T; (b) shift image u.

The results in figure 2 show that, generally, the shift image u features a lower UQI if compared to the transmission image T, in agreement with the behavior observed from the residuals in figure 1. Referring to figure 2(a), it can be noted that the UQI is a constant function of the sampling step, meaning that the quality of transmission images does not rely on illumination oversampling. As the only exception, the image quality drops only for the smallest window (3×3), coupled with the largest step. In contrast with the observations made for the transmission images, the quality of the shift images depends on the illumination sampling given by dx and on the size of the analysis window. Referring to figure 2 it can be observed that: (i) for $\mathrm{d}x \leqslant \Delta X/2$, the smallest window W (3×3) achieves the highest UQI value; (ii) for $\mathrm{d}x > \Delta X/2$, the quality of images significantly decreases for the smallest (3×3) window size. In this case, bigger windows (5×5) and (7×7) achieve the best match with the ground truth. To better explain this behavior, the actual reconstructions for a few different sampling steps are shown in figure 3. From figure 3 it can be observed how the choice of the shift dx affects the image quality. In particular, for a (3×3) window and step sizes $\mathrm{d}x > \Delta X/2 = 10\,\mu\mathrm{m}$, UMPA-1D introduces a bar pattern artifact that compromises the overall image quality. These artifacts, due to a sub-optimal sampling with the mask positions, can be mitigated by selecting a larger window in UMPA-1D. However, from the model's definition and the cost function (eqs. (2.1) and (2.2)), the weighted average within the window is expected to introduce a blur into the reconstructed images, thus reducing the noise at the cost of a loss in the spatial resolution and a reduced sensitivity in the shift image [8]. This is confirmed by figure 4, which compares the horizontal profiles passing from the center of the sphere for the ground truth, and two UMPA-1D reconstructions with different window sizes (3×3 and 7×7) for a well-sampled dataset (i.e., with $\mathrm{d}x = 10\,\mu\mathrm{m}$). The plots in figure 4 show that the smaller window (3×3) better matches the ground truth around the edges of the sphere (maximum and minimum values of the profiles). However, if compared to the larger window, it shows a larger dispersion around the ground truth values.

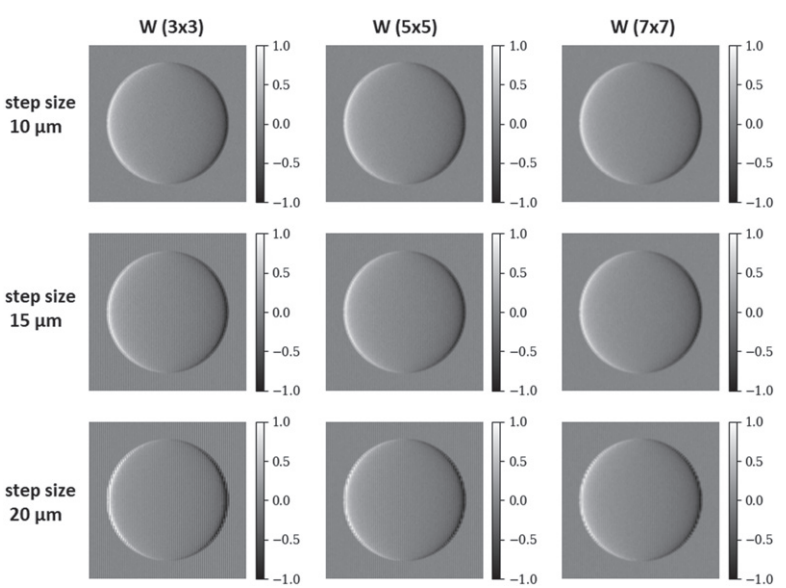

Figure 3. Shift images obtained considering different illumination samplings and reconstructed with different window sizes.

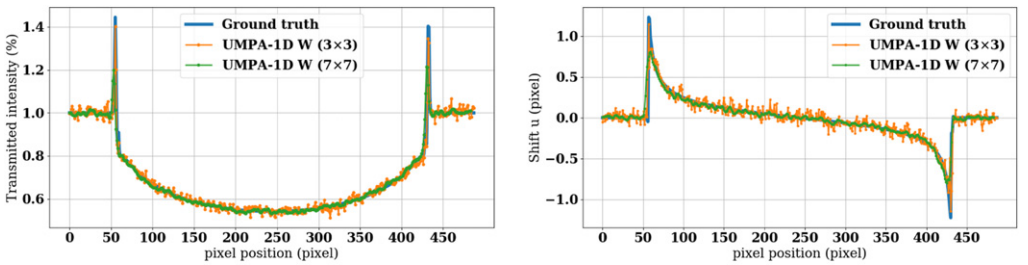

Figure 4. Horizontal profiles of the sample sphere extracted from UMPA-1D reconstructions with different window sizes (3 × 3) and (7 × 7), compared with the ground truth: (a) transmission T, (b) differential phase u.

A benchmark for UMPA-1D was run on a laptop with an 8-core Intel i7-11800H CPU. Runtime mean values and standard deviations were computed over five runs. The benchmark was repeated for different image sizes from (100 × 100) to (2000 × 2000). Using 4 threads, UMPA-1D was run with a (3 × 3) window on a dataset made by 12 steps with dx = 10 µm. The results are reported in table 1.

Table 1. Runtime measurement of UMPA-1D as a function of the image size. Each reconstruction refers to a dataset including 12 mask positions shifted with steps dx = 10 µm, using 4 threads and a (3 × 3) reconstruction window.

Image size (pixels)	100 × 100	500 × 500	1000 × 1000	1500 × 1500	2000 × 2000
recon. time (s)	0.004 ± 0.003	0.14 ± 0.02	0.90 ± 0.05	1.90 ± 0.05	3.40 ± 0.06

The UMPA-1D algorithm has been tested also for a realistic case, considering actual images of a plant specimen including flower buds. Figures 5(a)–(c) show the transmission, differential-phase, and dark-field images obtained with (3 × 3) window. Figure 5(d) shows the integrated-phase image, obtained from the differential-phase image with the algorithm described in [13].

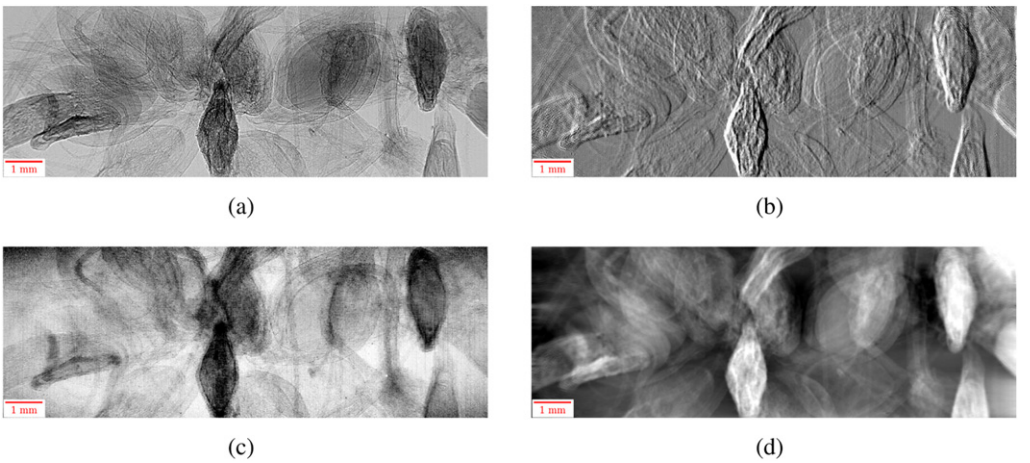

Figure 5. Images of a plant specimen with some flower buds acquired with an EI setup in beam-tracking mode, and reconstructed with UMPA-1D: (a) transmission T; (b) differential phase u; (c) dark-field D; (d) integrated phase. Images were reconstructed with a (3×3) window.

4 Conclusions

The UMPA algorithm provides a fast general solution for XPCI techniques making use of speckles or masks and acquisition procedures sensitive to refraction along both the vertical and the horizontal axes [9]. Compared with masks with 2D periodicity, 1D masks allow the collection of higher statistics with a single exposure, thus enabling faster XPCI scans. The extension of the original UMPA to the 1D case (UMPA-1D) expands the range of applications to EI and GI setups making use of 1D periodic masks directly resolved by the detection system. UMPA-1D provides a fast algorithmic solution with reconstruction times $\leqslant 0.9$ s for a 1000×1000 image (using $\geqslant 4$ threads), being particularly convenient for large tomographic datasets. The presented version of UMPA-1D, together with the simulation code employed for EI simulations, is made publicly available [14].

Acknowledgments

This work has received funding from the European Research Council (ERC) under the European Union's Horizon 2020 research and innovation programme under Grant Agreement No. 866026. PEPI project, funded by the Istiuto Nazionale di Fisica Nucleare (National Scientific Commission 5 for Technological and Interdisciplinary Research) Grant No. 22260/2020, is acknowledged.

References

[1] L. Quenot, S. Bohic and E. Brun, *X-ray phase contrast imaging from synchrotron to conventional sources: a review of the existing techniques for biological applications, Appl. Sci.* **12** (2022) 9539.

[2] W. Cong, F. Pfeiffer, M. Bech and G. Wang, *X-ray dark-field imaging modeling, J. Opt. Soc. Am. A* **29** (2012) 908.

[3] A. Olivo, *Edge-illumination X-ray phase-contrast imaging, J. Phys.: Condens. Matter* **33** (2021) 363002.

[4] F. Pfeiffer et al., *Hard-X-ray dark-field imaging using a grating interferometer, Nat. Mater.* **7** (2008) 134.

[5] S.K. Morgan, D.M. Paganin and K.K.W. Siu, *X-ray phase imaging with a paper analyzer, Appl. Phys. Lett.* **100** (2012) 124102.

[6] F.A. Vittoria et al., *Multimodal phase-based X-ray microtomography with nonmicrofocal laboratory sources, Phys. Rev. Appl.* **8** (2017) 064009.

[7] S. Berujon, H. Wang and K. Sawhney, *X-ray multimodal imaging using a random-phase object, Phys. Rev. A* **86** (2012) 063813.

[8] M.C. Zdora et al., *X-ray Phase-Contrast Imaging and Metrology through Unified Modulated Pattern Analysis, Phys. Rev. Lett.* **118** (2017) 203903.

[9] F. De Marco et al., *High-speed processing of X-ray wavefront marking data with the Unified Modulated Pattern Analysis (UMPA) model, Opt. Express* **31** (2023) 635.

[10] J.W. Goodman, *Introduction to Fourier Optics*, Roberts and Company Publishers (2005).

[11] C. Zuo et al., *Transport of intensity equation: a tutorial, Opt. Lasers Eng.* **135** (2020) 106187.

[12] Z. Wang and A.C. Bovik, *A universal image quality index, IEEE Signal Process. Lett.* **9** (2002) 81.

[13] L. Massimi, I. Buchanan, A. Astolfo, M. Endrizzi and A. Olivo, *Fast, non-iterative algorithm for quantitative integration of X-ray differential phase-contrast images, Opt. Express* **21** (2020) 39677.

[14] V. Di Trapani et al., *Unified Modulation Pattern Analysis (UMPA) algorithm for 1D sensitive X-ray phase contrast imaging techniques,* https://github.com/optimato/UMPA-1D.git Github (2022) (retrieved 19 December 2022).